Noninvasive holographic imaging through dynamically scattering media

Naoki Matsuda[1], **Jun Tanida**[2], **Makoto Naruse**[1], **and Ryoichi Horisaki**[1,*]

[1] *Department of Information Physics and Computing, Graduate School of Information Science and Technology, The University of Tokyo, 7-3-1 Hongo, Bunkyo-ku, Tokyo 113-8656, Japan*
[2] *Department of Information and Physical Sciences, Graduate School of Information Science and Technology, Osaka University, 1-5 Yamadaoka, Suita, Osaka 565-0871, Japan*
[*] *horisaki@g.ecc.u-tokyo.ac.jp*

Compiled December 20, 2023

We present a noninvasive method for quantitative phase imaging through dynamically scattering media. A complex amplitude object, illuminated with coherent light, is captured through a dynamically scattering medium and a variable coded aperture, without the need for interferometric measurements or imaging optics. The complex amplitude of the object is computationally retrieved from intensity images that use multiple coded aperture patterns, employing a stochastic gradient descent algorithm. We demonstrate the proposed method both numerically and experimentally.

http://dx.doi.org/10.1364/ao.XX.XXXXXX

Imaging through scattering media has long been a challenging issue in the fields of optics and photonics. Representative examples are looking inside biological tissue in life science and observing stars through the turbulent atmosphere in astronomy [1–3]. Various methods have been proposed for imaging through scattering media, based on feedback processes [4–7], transmission matrices [8, 9], and machine learning [10–13]. However, these methods primarily assume statically scattering media. For dynamically scattering media like biological tissue and atmospheric turbulence, speckle-correlation imaging is promising because it is a single-shot method and requires no calibration or training for scattering media [14–21].

Another approach for imaging through dynamically scattering media is the use of digital holography [22–25]. It measures interference patterns between optical fields from an object and a reference point light source, both of which are located behind a scattering medium. The object is reconstructed in the manner of digital holography. An advantage of this approach is the ability to image complex amplitude objects, which are not observable by speckle-correlation imaging because this technique assumes intensity objects. This advantage is important for stain-free visualization of transparent biomedical specimens. However, the reference point light source must be located behind a scattering medium. This setup is invasive and is not practically desirable.

In this paper, to address the above issue, we propose a noninvasive method for holographic or quantitative phase imaging of complex amplitude objects behind dynamically scattering two-dimensional media with no need for reference light. Not only the target complex amplitude field but also the characteristics of scattering media are estimated in the proposed method. This allows visualization of the object without prior information about the scattering media and offers practicality across a wide range of applications by means of lensless and interferometry-free compact hardware. We demonstrated the proposed method numerically and experimentally.

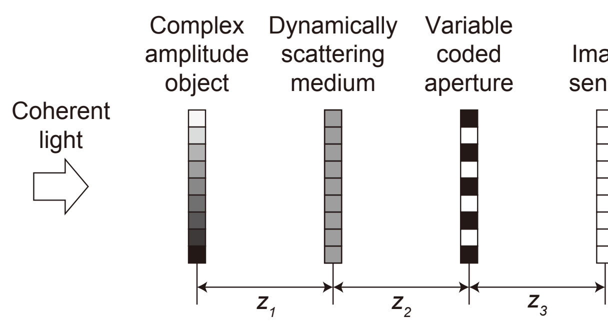

Fig. 1. Schematic diagram of the optical setup.

A schematic diagram of the optical setup of the proposed method is shown in Fig. 1, in which imaging optics or an interferometric setup are not necessary. Here, we consider the single lateral axis x and the depth axis z, while omitting the other lateral axis y, for the sake of simplicity. The propagating field from a complex amplitude object $\boldsymbol{o} \in \mathbb{C}^{N\times 1}$, where N is the pixel count along the x-axis, illuminated with coherent light is scattered by the dynamical lateral medium $\boldsymbol{d}_{m,t} \in \mathbb{C}^{N\times 1}$. The scattered field passes through the variable coded aperture $\boldsymbol{a}_m \in \mathbb{R}^{N\times 1}$. Then, the field propagating onto the image sensor is captured as an intensity image $\boldsymbol{i}_m \in \mathbb{R}^{N\times 1}$. Here, $m \in \{1, .., M\}$ is the index of mask patterns on the variable coded aperture, and $t \in \{1, .., T\}$ is the temporal index of the dynamical scattering. The distance between the object and the scattering medium is z_1, the distance between the scattering medium and the coded aperture is z_2, and the distance between the coded aperture and the image sensor is z_3.

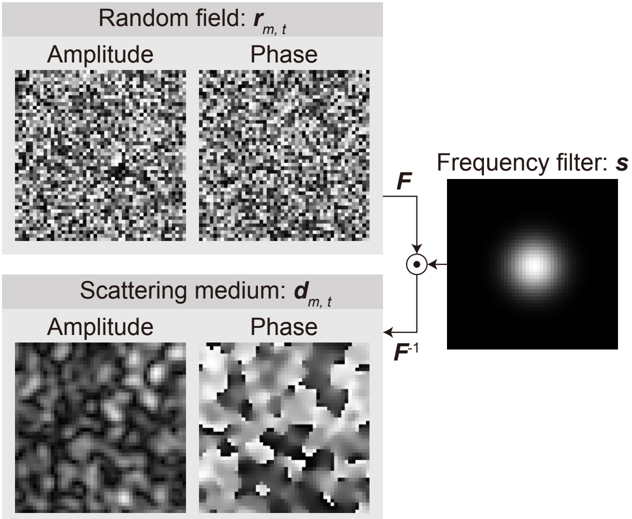

Fig. 2. Generation of the dynamically scattering medium with spatial frequency filtering.

This forward process is written with matrix operators as

$$\boldsymbol{i}_m = \frac{1}{T}\sum_{t=1}^{T} |\boldsymbol{g}_{m,t}|^2, \tag{1}$$

$$\boldsymbol{g}_{m,t} = \boldsymbol{P}_{z_3}\mathtt{diag}(\boldsymbol{a}_m)\boldsymbol{P}_{z_2}\mathtt{diag}(\boldsymbol{d}_{m,t})\boldsymbol{P}_{z_1}\boldsymbol{o}, \tag{2}$$

where $\boldsymbol{g}_{m,t} \in \mathbb{C}^{N\times 1}$ is the propagating complex amplitude field on the image sensor, and $\boldsymbol{P}_z \in \mathbb{C}^{N\times N}$ is the matrix representing the Fresnel propagation at distance z [26]. $\mathtt{diag}(\bullet)$ is an operator for generating a diagonal matrix, where the diagonal elements are the parenthesized vector, to implement the element-wise product of vectors. As shown in Eqs. (1) and (2), the T fields scattered by the dynamical medium $\boldsymbol{d}_{m,t}$ are ensemble averaged with sensor exposure or a computational process, and the M intensity images are obtained with the variable coded aperture $\boldsymbol{a}_m$.

We estimate not only the object $\boldsymbol{o}$ but also the characteristics of the dynamical scattering medium $\boldsymbol{d}_{m,t}$. In this study, the characteristics are assumed to be described by a spatial frequency filter $\boldsymbol{s} \in \mathbb{R}^{N\times 1}$ as shown in Fig. 2 and given by:

$$\boldsymbol{d}_{m,t} = \boldsymbol{F}^{-1}\mathtt{diag}(\boldsymbol{F}\boldsymbol{r}_{m,t})\boldsymbol{s}, \tag{3}$$

where $\boldsymbol{r}_{m,t} \in \mathbb{C}^{N\times 1}$ is a random complex amplitude field depending on the indices m and t. $\boldsymbol{F} \in \mathbb{C}^{N\times N}$ and $\boldsymbol{F}^{-1} \in \mathbb{C}^{N\times N}$ are the matrices representing the forward and inverse fast Fourier transforms, respectively. In this case, our estimation for the scattering-related variables is done only for $\boldsymbol{s}$, and not $\boldsymbol{d}_{m,t}$ or $\boldsymbol{r}_{m,t}$, because the captured intensity images $\boldsymbol{i}_m$ do not depend on $\boldsymbol{d}_{m,t}$ or $\boldsymbol{r}_{m,t}$ when T is sufficiently large. This is an advantage of the ensemble average of intensities of coherently scattered fields $\boldsymbol{g}_{m,t}$ along the t-dimension in Eq. (1).

We define the following error function e for the inverse problem of the forward process shown in Eqs. (1) and (2).

$$e = \frac{1}{M}\sum_{m=1}^{M} \|\boldsymbol{e}_m\|_2^2, \tag{4}$$

$$\boldsymbol{e}_m = \widehat{\boldsymbol{i}}_m - \boldsymbol{i}_m, \tag{5}$$

where $\boldsymbol{e}_m \in \mathbb{R}^{N\times 1}$ is the difference between the estimated intensity image $\widehat{\boldsymbol{i}}_m$, where $\widehat{\bullet}$ denotes the estimated variables in the inverse problem, and the captured intensity image $\boldsymbol{i}_m$, and $\|\bullet\|_2$ is the ℓ_2-norm. We solve the inverse problem by minimizing the error function e based on gradient descent with respect to the object $\widehat{\boldsymbol{o}}$ and the filter $\widehat{\boldsymbol{s}}$. The partial derivatives with respect to these two variables are written as

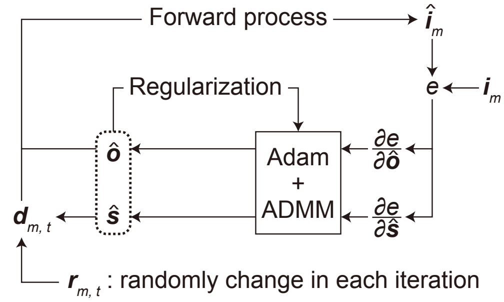

Fig. 3. Flow of the reconstruction process. $\boldsymbol{i}_m$: the captured intensity image. $\widehat{\boldsymbol{i}}_m$: the estimated intensity image. e: the error function. $\widehat{\boldsymbol{o}}$: the estimated object. $\widehat{\boldsymbol{s}}$: the estimated filter. $\boldsymbol{d}_{m,t}$: the dynamically scattering medium. $\boldsymbol{r}_{m,t}$: the random complex amplitude field.

$$\frac{\partial e}{\partial \widehat{\boldsymbol{o}}} = \frac{4}{MT}\sum_{m=1}^{M}\sum_{t=1}^{T} \boldsymbol{P}_{z_1}^H \mathtt{diag}(\boldsymbol{F}^{-1}\mathtt{diag}(\boldsymbol{F}\boldsymbol{r}_{m,t})\widehat{\boldsymbol{s}})^H \boldsymbol{P}_{z_2}^H \mathtt{diag}(\boldsymbol{a}_m)^H \boldsymbol{P}_{z_3}^H \mathtt{diag}(\boldsymbol{g}_{m,t})\boldsymbol{e}_m, \tag{6}$$

$$\frac{\partial e}{\partial \widehat{\boldsymbol{s}}} = \frac{4}{MT}\sum_{m=1}^{M}\sum_{t=1}^{T} \mathtt{real}[\mathtt{diag}(\boldsymbol{F}\boldsymbol{r}_{m,t})^H \boldsymbol{F}\mathtt{diag}(\boldsymbol{P}_{z_1}\widehat{\boldsymbol{o}})^H \boldsymbol{P}_{z_2}^H \mathtt{diag}(\boldsymbol{a}_m)^H \boldsymbol{P}_{z_3}^H \mathtt{diag}(\boldsymbol{g}_{m,t})\boldsymbol{e}_m], \tag{7}$$

where the superscript H denotes Hermitian conjugation, and $\mathtt{real}[\bullet]$ is the real part of the parenthesized complex vector.

We update the estimated object $\widehat{\boldsymbol{o}}$ and the estimated filter $\widehat{\boldsymbol{s}}$ with the partial derivatives in Eqs (6) and (7) by using the Adam optimizer as shown in Fig. 3 and given by:

$$\widehat{\boldsymbol{o}}_{k+1} = \widehat{\boldsymbol{o}}_k - \mathtt{Adam}\left[\frac{\partial e}{\partial \widehat{\boldsymbol{o}}_k}\right], \tag{8}$$

$$\widehat{\boldsymbol{s}}_{k+1} = \widehat{\boldsymbol{s}}_k - \mathtt{Adam}\left[\frac{\partial e}{\partial \widehat{\boldsymbol{s}}_k}\right], \tag{9}$$

where $k \in \mathbb{N}$ denotes the index of the iterations, and $\mathtt{Adam}[\bullet]$ is an operator of the Adam optimizer to calculate the updating steps with the derivatives and the momenta [27]. We additionally employ the total variation for regularizing the object $\widehat{\boldsymbol{o}}$ and the filter $\widehat{\boldsymbol{s}}$ by using the alternating direction method of multipliers (ADMM), as shown in Fig. 3 [28–30]. As mentioned above, the random field $\boldsymbol{r}_{m,t}$ for generating the dynamically scattering medium $\boldsymbol{d}_{m,t}$ in the inverse problem does not have to be identical to that in the actual measurement process due to the ensemble average in Eq. (1). Furthermore, in the inverse problem, we can set the number of ensemble averages T to a small value through the compressive propagation, where $\boldsymbol{r}_{m,t}$ randomly changes in each iteration based on stochastic gradient descent, and thus can reduce the computational cost of the inverse problem, as shown in Fig. 3 [31, 32].

We conducted a simulation to validate the proposed method. The amplitude and the phase of the object $\boldsymbol{o}$ shown in Figs. 4(a) and 4(b), respectively, were assumed in the simulation. These are the standard *peppers* image, and its 90 degrees-rotated version. Here, the pixel count N^2 was 128^2, the pixel pitch was

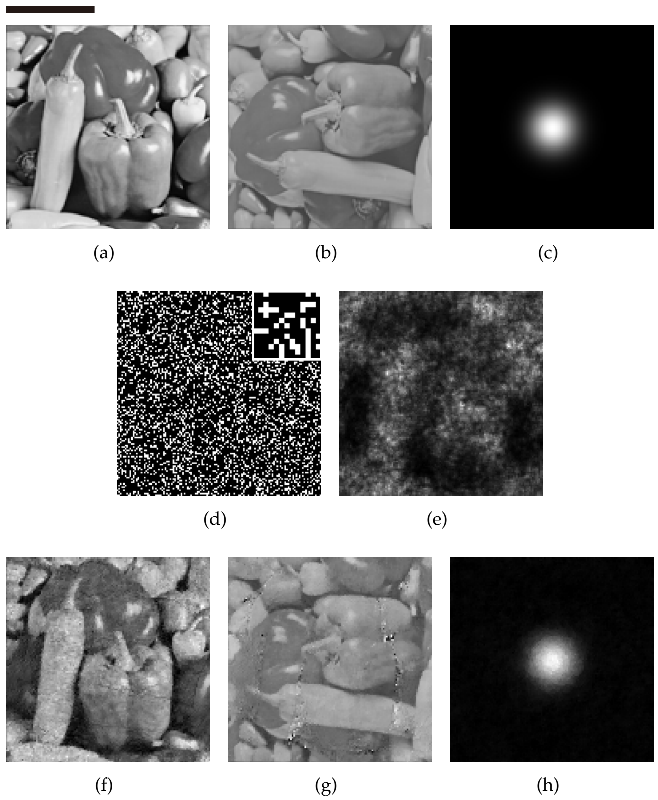

Fig. 4. Simulation results. (a) Amplitude and (b) phase of the object. (c) Spatial frequency filter. (d) An example of the variable coded aperture, where the inset illustrates a close-up of the mask pattern, and (e) its corresponding captured intensity image. (f) Amplitude and (g) phase of the reconstructed object. (h) Reconstruction of the spatial frequency filter. The scale bar in (a) is 2 mm. The phase images are normalized in the interval $[-\pi, \pi]$.

36 µm, and the wavelength of the illumination was 532 nm. All the distances z_1, z_2, and z_3 indicated in Fig. 1 were set to 5.0 cm. The spatial frequency filter $\boldsymbol{s}$ in the simulation is shown in Fig. 4(c). The number of mask patterns M on the variable coded aperture $\boldsymbol{a}_m$ was 10, and the mask patterns were set as uniform random binary distributions. One of the mask patterns is shown in Fig. 4(d). The number of ensemble averages T for the dynamically scattered fields was 100. One of the captured intensity images $\boldsymbol{i}_m$ is shown in Fig. 4(e), which corresponds to the mask pattern in Fig. 4(d).

In the reconstruction process, the number of ensemble averages T was set to 10, and the number of iterations was 10,000. The random field $\boldsymbol{r}_{m,t}$ randomly changed in each iteration. In the Adam optimizer, the learning rate was set to 0.01 for the object and 0.02 for the filter. The gradient decay factor was 0.9, and squared gradient decay factor was 0.95, for both the object and the filter [27]. The reconstructed amplitude and phase of the object is shown in Figs. 4(f) and 4(g), respectively. The root-mean-square error (RMSE) between the original and reconstructed fields was 0.14. The reconstructed filter is shown in Fig. 4(h), and the RMSE between the original and reconstructed filters was 0.042. Therefore, our method was numerically demonstrated.

We numerically verified the relationship between the number of mask patterns M on the variable coded aperture and the

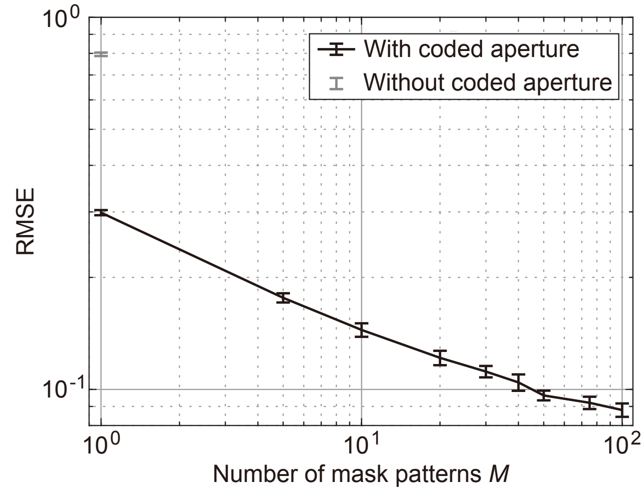

Fig. 5. Reconstruction errors calculated using the RMSE with the coded aperture for different numbers of mask patterns and without the coded aperture.

reconstruction error. Here, all the parameters were the same as those in the previous simulation except for the number of mask patterns. We also conducted a simulation without the coded aperture, under identical conditions to those used in the simulation with the coded aperture, to serve as a reference. The result is depicted in Fig. 5, where the centers and heights of the error bars represent the averages and standard deviations of the RMSEs from ten trials, each with a different mask pattern and random fields. As shown in the result, the reconstruction error was decreased by increasing the number of mask patterns. The reduction in reconstruction error through the use of the coded aperture was also verified.

We experimentally demonstrated the proposed method with the optical setup shown in Fig. 1. The complex amplitude object was implemented with a circular hole, partially covered by a cover glass and a slide glass. This object was illuminated by a collimated beam from a laser diode (DJ532-40 manufactured by Thorlabs, wavelength: 532 nm). The light passing through the object was dynamically scattered with a diffuser (KHYP1-12 manufactured by Optical Solutions, circular diffusion angle: 1°) that was moved randomly in directions perpendicular to the optical axis by a motorized stage (OSMS20-85 manufactured by OptoSigma). The scattered light was modulated by a variable coded aperture implemented with a transmissive spatial light modulator (LC2012 manufactured by HOLOEYE Photonics, pixel count: 1024×768, pixel pitch: 36 µm). The resultant light was captured by a monochromatic image sensor (DMK38UX253 manufactured by The Imaging Source, pixel count: 4096×3000, pixel pitch: 3.45 µm). The distances z_1, z_2, and z_3 in Fig. 1 were set to 4.3 cm, 5.0 cm, and 4.9 cm, respectively.

First, we removed the diffuser and measured the complex amplitude field of the object with a coded-aperture-based phase imaging method as a reference [33]. The reconstructed amplitude and phase of the object are shown in Figs. 6(a) and 6(b), respectively, where the partial phase shifts caused by the the glass plates are evident. Next, we executed the proposed method using the motorized diffuser. The number of coded mask patterns M was 10. One of the mask patterns is shown in Fig. 6(c). On each mask pattern, the diffuser was randomly displaced 100-times ($= T$), and the scattered light was captured. These

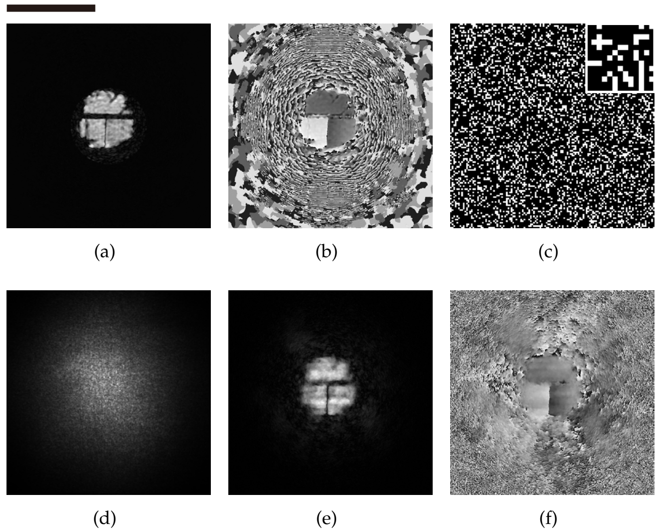

Fig. 6. Experimental results. (a) Amplitude and (b) phase of the object as a reference observed without the scattering medium. (c) An example of the variable coded aperture, where the inset illustrates a close-up of the mask pattern, and (d) its corresponding captured intensity image. (e) Amplitude and (f) phase of the reconstructed object. The scale bar in (a) is 2 mm. The phase images are normalized in the interval $[-\pi, \pi]$.

100 scattered intensity images were ensemble averaged. The averaged image is shown in Fig. 6(d), which corresponds to the mask pattern in Fig. 6(c). In practical scenarios, the averaging process can be substituted with integration over an exposure time that is longer than the temporal variance of the dynamically scattering media. For the reconstruction process, the number of iterations was set to 50,000. The learning rate was set to 0.03 for the object and 0.1 for the filter. The other parameters in the Adam optimizer were set to those in the original work [27]. A square support was placed on the spatial frequency filter of the scattering medium. The reconstructed amplitude and phase are shown in Figs. 6(e) and 6(f), respectively. The RMSE between the reference and reconstructed fields was 0.11. As shown in these results, we successfully demonstrated the proposed method.

In summary, we proposed a method for noninvasive holographic imaging of complex amplitude objects through dynamically scattering media. In the method, the object behind a dynamically scattering medium was illuminated with coherent light, and scattered light was captured through a variable coded aperture without any interferometer or reference light source. The amplitude and phase of the object, as well as the spatial frequency characteristics of the scattering medium, were estimated from multiple intensity images based on a stochastic descent algorithm. Our method was demonstrated through both simulation and experiment. In the latter, the optical setup was composed of a complex amplitude object created with glass plates, a dynamically scattering medium implemented with a randomly moving diffuser, and a variable coded aperture realized using a spatial light modulator.

Our method is noninvasive and simplifies the optical setup for holographic imaging through dynamically scattering media because imaging optics and reference light are not necessary. Future issues will be extending the method to more practical scenarios, for example, visualization of objects within scattering media and three-dimensional imaging through scattering media [16, 17, 20]. Due to its adaptability and simplicity, our proposed method is promising for various imaging applications, including fluorescence-label-free biomedical imaging and astronomical observations through atmospheric turbulence.

Funding. Japan Society for the Promotion of Science (JP20K05361, JP20H05890, JP23H01874, JP23H05444); Asahi Glass Foundation.

Disclosures. The authors declare no conflicts of interest.

Data availability. Data may be obtained from the authors upon reasonable request.

REFERENCES

1. R. H. Brown and R. Q. Twiss, Nature **177**, 27 (1956).
2. V. Ntziachristos, Nat. Methods **7**, 603 (2010).
3. R. Davies and M. Kasper, Annu. Rev. Astron. Astrophys. **50**, 305 (2012).
4. A. P. Mosk, A. Lagendijk, G. Lerosey, and M. Fink, Nat. Photonics **6**, 283 (2012).
5. G. Stern and O. Katz, Opt. Lett. **44**, 143 (2019).
6. A. Thendiyammal, G. Osnabrugge, T. Knop, and I. M. Vellekoop, Opt. Lett. **45**, 5101 (2020).
7. T. Yeminy and O. Katz, Sci. Adv. **7**, eabf5364 (2021).
8. S. Popoff, G. Lerosey, M. Fink, A. C. Boccara, and S. Gigan, Nat. Commun. **1**, 81 (2010).
9. A. Liutkus, D. Martina, S. Popoff, G. Chardon, O. Katz, G. Lerosey, S. Gigan, L. Daudet, and I. Carron, Sci. Reports **4**, 5552 (2014).
10. R. Horisaki, R. Takagi, and J. Tanida, Opt. Express **24**, 13738 (2016).
11. Y. Li, Y. Xue, and L. Tian, Optica **5**, 1181 (2018).
12. Y. Sun, J. Shi, L. Sun, J. Fan, and G. Zeng, Opt. Express **27**, 16032 (2019).
13. I. Kang, S. Pang, Q. Zhang, N. Fang, and G. Barbastathis, Opt. Express **29**, 5316 (2021).
14. J. Bertolotti, E. G. Van Putten, C. Blum, A. Lagendijk, W. L. Vos, and A. P. Mosk, Nature **491**, 232 (2012).
15. O. Katz, P. Heidmann, M. Fink, and S. Gigan, Nat. Photonics **8**, 784 (2014).
16. Y. Okamoto, R. Horisaki, and J. Tanida, Opt. Lett. **44**, 2526 (2019).
17. R. Horisaki, Y. Okamoto, and J. Tanida, Opt. Lett. **44**, 4032 (2019).
18. K. Ehira, R. Horisaki, Y. Nishizaki, M. Naruse, and J. Tanida, Appl. Opt. **60**, 2388 (2021).
19. D. Wang, S. K. Sahoo, X. Zhu, G. Adamo, and C. Dang, Nat. Commun. **12**, 3150 (2021).
20. Y. Endo, J. Tanida, M. Naruse, and R. Horisaki, Intell. Comput. (2022).
21. R. Mashiko, J. Tanida, M. Naruse, and R. Horisaki, Appl. Opt. **62**, 8327 (2023).
22. M. Paturzo, A. Finizio, P. Memmolo, R. Puglisi, D. Balduzzi, A. Galli, and P. Ferraro, Lab on a Chip **12**, 3073 (2012).
23. A. K. Singh, D. N. Naik, G. Pedrini, M. Takeda, and W. Osten, Opt. Express **22**, 7694 (2014).
24. A. S. Somkuwar, B. Das, R. Vinu, Y. Park, and R. K. Singh, JOSA A **34**, 1392 (2017).
25. S. Kodama, M. Ohta, K. Ikeda, Y. Kano, Y. Miyamoto, W. Osten, M. Takeda, and E. Watanabe, Appl. Opt. **58**, G345 (2019).
26. J. W. Goodman, *Introduction to Fourier Optics* (McGraw-Hill, 1996).
27. D. P. Kingma and J. Ba, arXiv preprint arXiv:1412.6980 (2014).
28. L. I. Rudin, S. Osher, and E. Fatemi, Phys. D: Nonlinear Phenom. **60**, 259 (1992).
29. C. Gaur, B. Mohan, and K. Khare, JOSA A **32**, 1922 (2015).
30. S. H. Chan, X. Wang, and O. A. Elgendy, IEEE Trans. on Comput. Imaging **3**, 84 (2016).
31. R. Horisaki, T. Aoki, Y. Nishizaki, A. Röhm, N. Chauvet, J. Tanida, and M. Naruse, Opt. Lett. **47**, 613 (2022).
32. R. Suda, M. Naruse, and R. Horisaki, Opt. Lett. **47**, 3844 (2022).
33. R. Horisaki, Y. Ogura, M. Aino, and J. Tanida, Opt. Lett. **39**, 6466 (2014).

FULL REFERENCES

1. R. H. Brown and R. Q. Twiss, "Correlation between photons in two coherent beams of light," Nature **177**, 27–29 (1956).
2. V. Ntziachristos, "Going deeper than microscopy: the optical imaging frontier in biology," Nat. Methods **7**, 603–614 (2010).
3. R. Davies and M. Kasper, "Adaptive optics for astronomy," Annu. Rev. Astron. Astrophys. **50**, 305–351 (2012).
4. A. P. Mosk, A. Lagendijk, G. Lerosey, and M. Fink, "Controlling waves in space and time for imaging and focusing in complex media," Nat. Photonics **6**, 283–292 (2012).
5. G. Stern and O. Katz, "Noninvasive focusing through scattering layers using speckle correlations," Opt. Lett. **44**, 143–146 (2019).
6. A. Thendiyammal, G. Osnabrugge, T. Knop, and I. M. Vellekoop, "Model-based wavefront shaping microscopy," Opt. Lett. **45**, 5101–5104 (2020).
7. T. Yeminy and O. Katz, "Guidestar-free image-guided wavefront shaping," Sci. Adv. **7**, eabf5364 (2021).
8. S. Popoff, G. Lerosey, M. Fink, A. C. Boccara, and S. Gigan, "Image transmission through an opaque material," Nat. Commun. **1**, 81 (2010).
9. A. Liutkus, D. Martina, S. Popoff, G. Chardon, O. Katz, G. Lerosey, S. Gigan, L. Daudet, and I. Carron, "Imaging with nature: compressive imaging using a multiply scattering medium," Sci. Reports **4**, 5552 (2014).
10. R. Horisaki, R. Takagi, and J. Tanida, "Learning-based imaging through scattering media," Opt. Express **24**, 13738–13743 (2016).
11. Y. Li, Y. Xue, and L. Tian, "Deep speckle correlation: a deep learning approach toward scalable imaging through scattering media," Optica **5**, 1181–1190 (2018).
12. Y. Sun, J. Shi, L. Sun, J. Fan, and G. Zeng, "Image reconstruction through dynamic scattering media based on deep learning," Opt. Express **27**, 16032–16046 (2019).
13. I. Kang, S. Pang, Q. Zhang, N. Fang, and G. Barbastathis, "Recurrent neural network reveals transparent objects through scattering media," Opt. Express **29**, 5316–5326 (2021).
14. J. Bertolotti, E. G. Van Putten, C. Blum, A. Lagendijk, W. L. Vos, and A. P. Mosk, "Non-invasive imaging through opaque scattering layers," Nature **491**, 232–234 (2012).
15. O. Katz, P. Heidmann, M. Fink, and S. Gigan, "Non-invasive single-shot imaging through scattering layers and around corners via speckle correlations," Nat. Photonics **8**, 784–790 (2014).
16. Y. Okamoto, R. Horisaki, and J. Tanida, "Noninvasive three-dimensional imaging through scattering media by three-dimensional speckle correlation," Opt. Lett. **44**, 2526–2529 (2019).
17. R. Horisaki, Y. Okamoto, and J. Tanida, "Single-shot noninvasive three-dimensional imaging through scattering media," Opt. Lett. **44**, 4032–4035 (2019).
18. K. Ehira, R. Horisaki, Y. Nishizaki, M. Naruse, and J. Tanida, "Spectral speckle-correlation imaging," Appl. Opt. **60**, 2388–2392 (2021).
19. D. Wang, S. K. Sahoo, X. Zhu, G. Adamo, and C. Dang, "Non-invasive super-resolution imaging through dynamic scattering media," Nat. Commun. **12**, 3150 (2021).
20. Y. Endo, J. Tanida, M. Naruse, and R. Horisaki, "Extrapolated speckle-correlation imaging," Intell. Comput. (2022).
21. R. Mashiko, J. Tanida, M. Naruse, and R. Horisaki, "Extrapolated speckle-correlation imaging with untrained deep neural network," Appl. Opt. **62**, 8327–8333 (2023).
22. M. Paturzo, A. Finizio, P. Memmolo, R. Puglisi, D. Balduzzi, A. Galli, and P. Ferraro, "Microscopy imaging and quantitative phase contrast mapping in turbid microfluidic channels by digital holography," Lab on a Chip **12**, 3073–3076 (2012).
23. A. K. Singh, D. N. Naik, G. Pedrini, M. Takeda, and W. Osten, "Looking through a diffuser and around an opaque surface: a holographic approach," Opt. Express **22**, 7694–7701 (2014).
24. A. S. Somkuwar, B. Das, R. Vinu, Y. Park, and R. K. Singh, "Holographic imaging through a scattering layer using speckle interferometry," JOSA A **34**, 1392–1399 (2017).
25. S. Kodama, M. Ohta, K. Ikeda, Y. Kano, Y. Miyamoto, W. Osten, M. Takeda, and E. Watanabe, "Three-dimensional microscopic imaging through scattering media based on in-line phase-shift digital holography," Appl. Opt. **58**, G345–G350 (2019).
26. J. W. Goodman, *Introduction to Fourier Optics* (McGraw-Hill, 1996).
27. D. P. Kingma and J. Ba, "Adam: a method for stochastic optimization," arXiv preprint arXiv:1412.6980 (2014).
28. L. I. Rudin, S. Osher, and E. Fatemi, "Nonlinear total variation based noise removal algorithms," Phys. D: Nonlinear Phenom. **60**, 259–268 (1992).
29. C. Gaur, B. Mohan, and K. Khare, "Sparsity-assisted solution to the twin image problem in phase retrieval," JOSA A **32**, 1922–1927 (2015).
30. S. H. Chan, X. Wang, and O. A. Elgendy, "Plug-and-play admm for image restoration: fixed-point convergence and applications," IEEE Trans. on Comput. Imaging **3**, 84–98 (2016).
31. R. Horisaki, T. Aoki, Y. Nishizaki, A. Röhm, N. Chauvet, J. Tanida, and M. Naruse, "Compressive propagation with coherence," Opt. Lett. **47**, 613–616 (2022).
32. R. Suda, M. Naruse, and R. Horisaki, "Incoherent computer-generated holography," Opt. Lett. **47**, 3844–3847 (2022).
33. R. Horisaki, Y. Ogura, M. Aino, and J. Tanida, "Single-shot phase imaging with a coded aperture," Opt. Lett. **39**, 6466–6469 (2014).